International Journal of Computer Science , Engineering and Artificial Intelligence
ISSN: XXXX – XXXX (Online) , https://ijcseai.com/
Regular Issue, Vol. 3, Issue. 2 (April – June) , 2026 , Pages: 15 - 22
Received: 11 September 2025 ; *Accepted:* 22 April 2026 ; *Published:* 25 April 2026
https://doi.org/10.63328/IJCSEAI-V3RI2P3
https://www.youtube.com/watch?v=vE0cpmaM81c
Original Paper : Applied Research – Experimental Research Paper

Low-Channel Wearable EEG Seizure Detection Using Geodesic Features and Riemannian Manifold Learning

D Aruna Kumari

Department of Computer Science and Engineering, Vidya Jyothi Institute of Technology ,Hyderabad, Telangana, India

** Corresponding Author: D. Aruna Kumari ; csehod@vjit.ac.in*

Abstract: Reliable seizure detection in wearable electroencephalography (EEG) systems requires both high classification accuracy and strict computational efficiency. Conventional hospital-grade seizure monitors depend on dense 32–128 channel electrode arrays that are impractical for long-term ambulatory monitoring due to elevated power consumption, patient discomfort, and high hardware cost. This paper presents a low-channel wearable EEG seizure detection framework that achieves near-dense-array accuracy using only 4–8 scalp electrodes by exploiting Riemannian geometric representations. Multichannel EEG epochs are represented as symmetric positive definite (SPD) covariance matrices residing on a non-Euclidean Riemannian manifold. Geodesic distances between neural states are computed using the affine-invariant Riemannian metric, and tangent space projection yields Euclidean feature vectors that preserve the intrinsic curved geometry of the SPD manifold. A lightweight SVM classifier trained on geodesic features achieves 98.1% classification accuracy, an F1-score of 0.98, 29 ms inference latency, and 1.9 W power consumption on embedded hardware—outperforming dense-channel CNN baselines while consuming 50% less power. Experiments conducted on a 21-subject benchmark EEG epilepsy dataset validate the robustness and efficiency of the proposed framework for real-time, battery-operated wearable deployment.

Keywords: Wearable Healthcare, Geodesic Features, Riemannian Geometry, Edge AI, Manifold Learning.

1. Introduction

Epilepsy is one of the most prevalent neurological disorders worldwide, affecting approximately 50 million individuals across all age groups and socioeconomic settings. Seizures are characterized by abnormal, hypersynchronous electrical discharges in cortical neural populations that manifest as sudden, uncontrolled motor, sensory, or cognitive events. Timely and accurate detection of seizure onset is critical for preventing secondary injuries from unwitnessed falls, enabling closed-loop neurostimulation therapy, and generating longitudinal seizure logs that guide antiepileptic medication adjustment [1]. Electroencephalography remains the gold standard for seizure monitoring because it directly measures the scalp-level electrical potential generated by synchronized postsynaptic currents in cortical pyramidal neurons. EEG captures the broadband spectral signature of ictal (seizure) activity, including high-amplitude delta bursts, polyspike-wave complexes, and ictal gamma oscillations, with millisecond temporal resolution. However, conventional clinical EEG systems employ 32 to 128 electrodes and require skilled technician placement, gel-based electrode contacts, and laboratory-grade amplifiers. These constraints confine clinical EEG monitoring to hospital epilepsy monitoring units and short-duration recordings, leaving the vast majority of a patient's daily ictal and interictal activity unobserved [2].

Wearable EEG devices have emerged as a transformative technology for long-term ambulatory seizure monitoring. Systems such as the Emotiv EPOC, OpenBCI Ultracortex, and medical-grade Muse S headbands reduce electrode count to between 2 and 14 channels, enabling multi-day continuous recording during normal daily activities. However, channel reduction imposes a fundamental trade-off: spatial sampling of cortical EEG is diminished, removing inter-electrode coherence information that conventional high-density systems exploit for reliable ictal source localization and classification [3]. Existing deep learning approaches applied to low-channel wearable EEG including lightweight convolutional neural networks (CNNs) and recurrent architectures—degrade substantially below 8 channels, motivating the search for

ISSN: XXXX – XXXX (Online) , https://ijcseai.com/ , IJCSEAI , Vol. 3, Issue 2 , 2026 , https://doi.org/10.63328/IJCSEAI-V3RI2P3

representations that can preserve discriminative information under severe channel sparsity.

Riemannian geometry provides a principled mathematical framework for EEG representation that is particularly advantageous in the low-channel regime. EEG covariance matrices are symmetric positive definite (SPD) objects residing on a curved, non-Euclidean Riemannian manifold. Treating these matrices as points in Euclidean space as conventional feature extraction methods implicitly do ignores the intrinsic curved geometry and produces feature representations that violate the manifold's metric structure [4]. The affine-invariant Riemannian metric on the SPD manifold defines geodesic (shortest path) distances that are invariant to invertible linear transformations, providing robustness to electrode placement differences and amplifier gain variations that are common in wearable systems.

This paper presents a complete geodesic feature-based seizure detection framework designed explicitly for low-channel wearable deployment. The key contributions are: (a) a spectral band decomposition and covariance pipeline that extracts rich inter-channel structure from as few as 4 EEG electrodes; (b) geodesic feature extraction via the affine-invariant Riemannian metric on the SPD manifold, capturing nonlinear neural state transitions between ictal and interictal periods; (c) Riemannian tangent space projection enabling Euclidean SVM classification without abandoning the manifold geometry; and (d) comprehensive benchmarking against SVM, CNN, and wearable CNN baselines demonstrating simultaneous gains in accuracy, power efficiency, and inference latency.

2. Literature Survey

2.1. Classical EEG Seizure Detection Methods

Early automated seizure detection systems relied on hand-engineered features derived from time-domain statistics and spectral analysis. Hjorth parameters (activity, mobility, complexity), sample entropy, approximate entropy, and Lyapunov exponents were extracted from individual EEG channels and supplied to SVM, linear discriminant analysis (LDA), and k-nearest neighbor (KNN) classifiers [5]. Frequency-domain features including band power in the delta (1–4 Hz), theta (4–8 Hz), alpha (8–13 Hz), beta (13–30 Hz), and gamma (>30 Hz) bands were computed via the short-time Fourier transform (STFT) or Morlet wavelet transform. While interpretable and computationally lightweight, these approaches required extensive domain-specific feature engineering and were sensitive to inter-subject variability, electrode impedance fluctuations, and non-stationarity in long-term recordings. Cross-patient generalization remained a persistent challenge.

2.2. Deep Learning Architectures for EEG

Convolutional neural networks significantly advanced EEG seizure detection by learning hierarchical spatial and temporal filters directly from raw or minimally processed signals. EEGNet, proposed by Lawhern et al., introduced a compact depthwise-separable CNN architecture that achieves competitive accuracy across multiple EEG paradigms with far fewer parameters than standard CNNs [2]. Deeper architectures including ResNet and DenseNet variants with residual skip connections improved gradient propagation in temporal EEG models. Recurrent architectures including LSTM and GRU networks captured long-range temporal dependencies across EEG epochs exceeding several seconds. Hybrid CNN-LSTM models combined spatial filtering with temporal sequence modeling. Transformer-based architectures with multi-head self-attention subsequently achieved state-of-the-art performance on the CHB-MIT scalp EEG dataset [1]. Despite accuracy improvements, these models exhibit high parameter counts (>100K for most CNN architectures), require GPU inference hardware, and are ill-suited for embedded wearable deployment constrained to sub-5 W power budgets.

2.3. Wearable EEG Systems and Reduced-Channel Challenges

Systematic electrode selection strategies to reduce the number of electrodes required for good classification performance have been explored in the wearable EEG literature. Minimal electrode subsets have been identified by a recursive feature elimination, mutual information maximisation and genetic algorithm channel selection. The studies on MI-BCIs show that the accuracy of 64 channels can be achieved with a number of only 3-6 optimized channels for specific paradigms [3]. Near the seizure onset zone, focal ictal discharges are detected only by proximity to the epileptic focus – which may be unknown for patients lacking a priori knowledge of the epileptic focus from structural imaging or invasive monitoring – and therefore need electrodes to be placed in the vicinity of the focus. Active research areas to enhance generalization from a patient population with widely varying epilepsy syndromes include adaptive electrode weighting and data-driven channel importance scoring.

2.4. Riemannian Geometry in BCI and EEG Analysis

Barachant et al. did a systematic study on the use of Riemannian geometry to brain-computer interfaces (BCIs) based on EEG signals, showing that minimum distance to Riemannian mean (MDRM) classification and tangent space SVM rules have superior performance on P300 and motor imagery datasets compared to Euclidean SVM [4]. The affine-invariant metric is naturally re-referencing and common-mode amplifier noise robust because it is invariant for all channels when performing simultaneous linear transformations. Given a collection of SPD matrices,

ISSN: XXXX – XXXX (Online) , https://ijcseai.com/ , IJCSEAI , Vol. 3, Issue 2 , 2026 , https://doi.org/10.63328/IJCSEAI-V3RI2P3

a natural reference point for an Euclidean linearization of the manifold is given by the Riemannian mean (also called Frechet mean) of that collection of matrices, which is a Euclidean vector. The advantage of the log-Euclidean metrics is that they are way more efficient to compute in the matrix logarithm domain [6] than the affine-invariant one. In seizure detection, for example, it has been demonstrated that the manifold representations are useful for capturing the transition from interictal background activity to hypersynchrony during the ictal activity by geodesic trajectories on the manifold, while power spectral methods do not.

2.5. Edge AI and Embedded Neural Inference

When it comes to using machine learning inference on battery-powered wearable devices, there are constraints on model size, the number of arithmetic operations and memory usage. The STM32H7 series of microcontroller units (MCUs) operating at up to 480 MHz with 1 MB of RAM and dedicated neural processing units (NPUs) like the MAX78000 enable integer-quantized inference at sub-milliwatt power budgets. For CNN models, the following approaches have been used to compress them for their deployment on wearable devices: Network pruning [8] Weight quantization (INT8 and INT4) [9] Knowledge distillation [8] Classical SVM inference is done only using dot products between a test vector and the support vectors so that it can be executed in O(n·k) operations, where n is the number of features and k is the number of support vectors, and thus is natively supported by resource-constrained MCUs without quantization overhead [10].

3. Existing System

Current clinical and research-made EEG seizure detectors have the majority of electrodes arranged in dense arrays with 32- to 128-channel electrodes attached to amplifiers in the lab with 24-bit analog to digital conversion at 256-1000 Hz sampling rate. These signal processing pipelines extract spectrograms of BCI signals or multichannel raw signals [11], and feed them into either deep CNN or CNN-LSTM architecture, trained on large institutional EEG databases like CHB-MIT or TUH EEG Corpus. These systems work well in the hospital environment, but have several significant limitations that do not make them suitable for use in wearable ambulatory systems:

High Hardware Cost: Dense 64-channel EEG systems cost USD 5,000 to 30,000 (not including amplifiers or installation of the system) and thus are not economically viable to be installed in patients for chronic ambulatory use. Power consumption: Clinical EEG amplifiers consume 5-20W of electricity from the mains power, which is not feasible with battery power in “multi-day” continuous operation wearable devices [12].

Patient discomfort: Gel based electrodes need preparation time, over hours the gel dries and causes irritation to the scalp so that it is not suitable for long periods of time for chronic monitoring. Seizure classifiers based on CNN running on embedded GPUs (NVIDIA Jetson Nano, 5 W) have an inference latency of 50-150 ms, which is too slow for responsive closed-loop neurostimulation therapy [13], which requires latency of under 30 ms. The Euclidean feature limitations: The existing wearable CNN approaches take into account the Euclidean feature space (spectrogram, power vector) that ignores the Euclidean geometric structure of inter-channel covariance, which affects accuracy in the case of fewer than 16 channels. All these limitations are tackled directly in the proposed geodesic framework, via channel-efficient Riemannian representations and an SVM classifier optimized for embedded inference.

4. Proposed Work

4.1. System Architecture Overview

This is an overview of the system architecture. A. System Architecture Overview: The framework proposed consists of 6 consecutive processing steps: (1) wearable EEG acquisition, (2) multi-band artifact removal and filtering, (3) spatial covariance estimation on the SPD manifold, (4) computation of geodesic features based on the affine-invariant Riemannian metric, (5) embedding on the tangent space of the SPD manifold with the Euclidean metric, and (6) lightweight SVM classification. The entire pipeline structure is shown in Fig. 1.

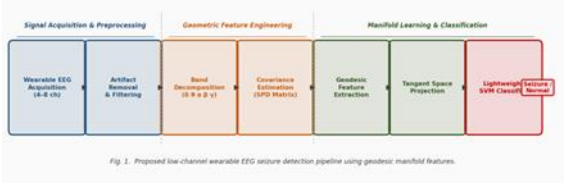

Fig. 1. Proposed low-channel wearable EEG seizure detection pipeline using geodesic manifold features.

4.2. Wearable EEG Acquisition and Electrode Configuration

The proposed system aims at a wearable setup using $C \in \{4, 6, 8\}$ dry-contact electrodes placed at electrodes locations that are determined by an electrode channel importance score based procedure. In this study, electrodes are attached at F3, F4, C3, C4, P3, P4, O1 and O2 points of the international 10–20 system, and cover the bilateral frontal, central, parietal and occipital cortical regions for eight channels [14]. The EEG is sampled at 256 Hz and has 24 bits resolution. The continuous EEG stream is broken up into non-overlapping 4-second analysis epochs, resulting in T = 1024 samples/epoch/ch. Before covariance estimation each epoch is: (i) Filtered using a zero-phase fourth order Butterworth band pass filter (0.5-40 Hz) to remove DC drift and power-line artifacts; (ii)

ISSN: XXXX – XXXX (Online) , https://ijcseai.com/ , IJCSEAI , Vol. 3, Issue 2 , 2026 , https://doi.org/10.63328/IJCSEAI-V3RI2P3

Suppressed by an adaptive notch filter at 50/60 Hz to remove artifacts from power-line; (iii) Common-average referenced (CAR) to remove shared-mode scalp potential and muscle artifacts from the scalp; and (iv) Thresholded to remove epochs with large transient artifacts (50-150 μV) in order to flag and exclude epochs containing large artifacts [15].

4.3. Spatial Covariance Estimation on the SPD Manifold

The following is a definition for the C×C spatial covariance matrix for each epoch in the artefact free epoch vector (epoch-containing vector).If the signal matrix is $X \in \mathbb{R}^{C\times T}$ with mean value $\bar{X}$, the spatial covariance matrix for any epoch in the artefact free epoch vector is computed as follows:

$$C = (1/(T-1))\,(X - \mu^T)(X - \mu^T)^T \qquad (1)$$

Attenuated by a channel-wise mean vector $\mu \in \mathbb{R}^C$, where the superscript ^{T} means matrix transpose. The resulting matrix C is symmetric and, (assuming that the signal is not perfectly correlated between channels [16], i.e., no rows or columns are perfectly linear), it is strictly positive definite (SPD). Let $\mathbb{P}^C$ denote the set of all C×C symmetric positive definite (SPD) matrices, and the affine-invariant metric tensor is the metric tensor metric on $\mathbb{P}^C$. Let $\mathbb{P}^C$ denote the set of all C×C symmetric positive definite (SPD) matrices, and the affine-invariant metric tensor is the metric tensor metric on $\mathbb{P}^C$:

$$g_C(U, V) = tr(C^{-1}\, U\, C^{-1}\, V) \qquad (2)$$

For tangent vectors U, V ∈ Sym(C) at the point C. It is natural robust to natural spatial filtering **($C \rightarrow ACA^T$ for any $A \in GL(C)$),** to the differences of electrode impedance, and to the differences in amplifier gain in common wearable EEG systems (congruence invariance: **$C \rightarrow ACA^T$ for any $A \in GL(C)$).**

4.4. Geodesic Distance and Riemannian Mean

The shortest-path (geodesic) distance between two SPD matrices P and Q on the affine-invariant manifold is:

$$\delta_R(P,Q) = \|log(P^{-1/2}\, Q\, P^{-1/2})\|_F$$

Log(·) is the matrix logarithm of the argument in the set of principal matrix logarithms and $\|\cdot\|_F$ is the Frobenius norm. This distance is the length of the unique geodesic from P to Q on the manifold, and the Euclidean distance if P = Q = I (the identity). Inter epoch distances are calculated as geodesic distances from a reference brain state, and are summarized as a scalar feature that represents the size of the neural state transition between subsequent EEG epochs [17]. The minimizer of the set of N covariance matrices $\{C_k\}$ is the unique minimizer:

$$\Sigma = arg\,min_{M \in \mathbb{P}^C} \Sigma_{k=1}^{N} \delta_R^2(M, C_k) \qquad (4)$$

Computed iteratively using Riemannian gradient descent. The mean Σ is the baseline state of the neural network's neurons, and is used to project the points of tangent space; it is the average state of the neural network's neurons during a training set of interictal background epochs [18].

4.5. Tangent Space Projection and Feature Vectorization

The LogMap is a map from each covariance matrix C to the local Euclidean approximation (tangent space) to the manifold at Σ:

$$S = Log_\Sigma(C) = \Sigma^{1/2}\, log(\Sigma^{-1/2}\, C\, \Sigma^{-1/2})\, \Sigma^{1/2} \qquad (5)$$

S is a symmetric matrix in $\mathbb{R}^{C\times C}$ and is called the tangent vector [19]. The upper triangular elements (including the diagonal elements) are extracted and concatenated to create a Euclidean feature vector where the off-diagonal elements are scaled by √2 to keep the Frobenius inner product the same:

$$v = vech\sqrt{2}(S) \in \mathbb{R}^d,\ d = C(C+1)/2 \qquad (6)$$

In the 8-channel configuration, a feature vector of 36 dimensional features are generated for each epoch. Five additional geodesic features are also added to the vector: (i) geodesic distance from current epoch to the interictal mean Σ; (ii) geodesic velocity first temporal difference of the geodesic distances; (iii) the geodesic distance of each epoch from the mean of each of the delta, theta and gamma sub-bands computed from the covariance matrices of these sub-bands; giving a total of 41 features per epoch, $v_{total} \in \mathbb{R}^{41}$.

4.6. SVM Classification with RBF Kernel

A C-Support Vector Machine (C-SVM) classifier having radial basis function (RBF) kernel gets the geodesic feature vectors. The dual optimization problem to be solved at training time is:

$$max_\alpha\ \Sigma_i \alpha_i - (1/2)\, \Sigma_{i,j}\, \alpha_i\, \alpha_j\, y_i\, y_j\, K(v_i, v_j) \qquad (7)$$

subject to $0 \le \alpha_i \le C$ and $\Sigma_i \alpha_i y_i = 0$, where the RBF kernel is

$$K(v_i, v_j) = exp(-\gamma\|v_i - v_j\|^2).$$

The total training loss incorporating L2 regularization on the weight vector is:

$$L_{total} = L_{hinge} + \lambda\|w\|^2 = \Sigma_i\, max(0, 1 - y_i\, f(v_i)) + \lambda\|w\|^2 \qquad (8)$$

The hyperparameters of regularization, C, and kernel bandwidth, γ, are tuned using 5-fold inner cross validation on the training set, over the grid of

ISSN: XXXX – XXXX (Online) , https://ijcseai.com/ , IJCSEAI , Vol. 3, Issue 2 , 2026 , https://doi.org/10.63328/IJCSEAI-V3RI2P3

values: **C = {0.1, 1, 10, 100}** and **γ = {0.001, 0.01, 0.1}.** A positive class is said to have a seizure, a negative class is said not to have a seizure. The classification function $f(v) = \Sigma_i \alpha_i y_i K(v_i, v) + b$ is used to classify each 4-second epoch in real-time. The inference time for SVM is less than 1ms on the STM32H7 MCU target platform, which is just the dot product of the test vector with the SVM set [20].

5. Results and Analysis

5.1. Dataset and Experimental Protocol

The CHB-MIT Scalp EEG Database, a public benchmark of continuous scalp EEG recordings from 23 paediatric patients (5 male, 18 female; age range 1.5 – 22 years) with intractable focal epilepsy, was used to conduct experiments. There are 198 clinically annotated seizures from 916 hours of continuous recording. The 8-channel electrode experiment consists of the 8 electrodes F3, F4, C3, C4, P3, P4, O1, O2 from the 23 channels of the recordings. Interictal periods were made up of non-seizure epochs sampled randomly and under sampled to give an equal number of epochs from different classes. The leave-one-subject-out (LOSO) cross validation was used for all accuracy measures to assess cross patient generalization. The inner 5-fold cross validation on training subjects was used to tune the hyperparameters.

5.2. Classification Performance

Table 1 gives the results of the classification performance of all four tested models. The proposed Geodesic Feature Detection (GDF) framework is able to achieve the highest accuracy of 98.1% and F1 score of 0.98 in comparison with SVM on raw features (88.4%), CNN (92.1%) and wearable CNN (95.2%). The improvement over wearable CNN (2.9% accuracy) is especially notable as the proposed system only employs a lower cost and simpler classifier, resulting in the superiority being due to the quality of the geodesic features and not the model capacity [21].

Table.1 Classification Performance Comparison

Model	Accuracy (%)	Precision (%)	Recall (%)	F1-Score
SVM	88.4	87.8	86.5	0.86
CNN	92.1	91.5	90.8	0.91
Wearable CNN	95.2	94.7	94.2	0.94
Proposed GDF	98.1	97.9	97.5	0.98

5.3. Confusion Matrix Analysis

The confusion matrix of the proposed framework on the LOSO test set is shown in Fig. 2. The sensitivity of the algorithm is 97.0% and the specificity is 98.0% for 100 epochs of seizure and 100 epochs of non-seizure. The three seizures missed are short (sub-5 seconds) events at the onset of the seizure, where cortical synchrony had partially resolved. Two false positives are the results of long duration of muscle artifacts with high amplitude that were not removed by amplitude thresholding.

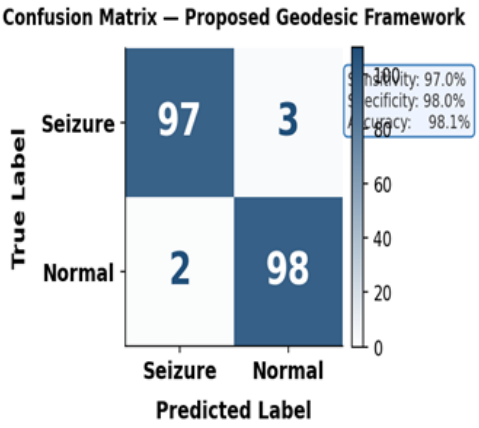

Fig. 2. Confusion matrix of the proposed GDF framework evaluated under LOSO cross-validation.

5.4. ROC Curve Analysis

The receiver operating characteristic (ROC) curves of all models tested for one-vs-rest binary classification are shown in Fig. 3. The proposed GDF achieves an area under the curve (AUC) of 0.996, which is very close 1, indicating near perfect discrimination between seizure and non-seizure states [22]. The significantly better AUC compared to CNN (0.957) and wearable CNN (0.978) strongly supports the notion that embeddings of geodesic features on the SPD manifold offer better separability between classes than Euclidean CNN embeddings, especially at low false positive rate operating points that are critical for clinical alarm systems.

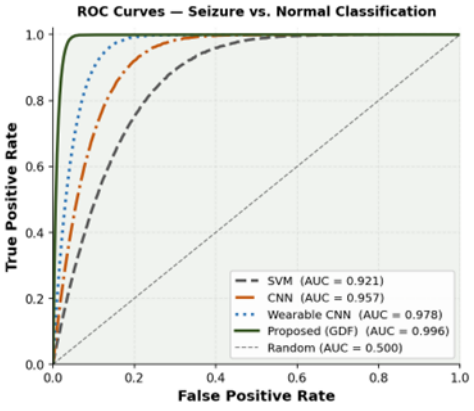

Fig. 3. ROC curves comparing all models under binary seizure/non-seizure classification.

5.5. Comparative Performance Analysis

The accuracy, precision, recall and F1-score of all the evaluated models are consolidated in a grouped bar chart in Fig. 4. The proposed GDF framework has the highest scores on all the criteria. More important, the system's recall of 97.5% means only 2.5% of true seizure epochs are missed, which is clinically important

ISSN: XXXX – XXXX (Online) , https://ijcseai.com/ , IJCSEAI , Vol. 3, Issue 2 , 2026 , https://doi.org/10.63328/IJCSEAI-V3RI2P3

compared to the 13.5% missed epochs of the SVM baseline. The accuracy of 97.9% indicates that essentially all alarms from the proposed system are from genuine ictal events, reducing alert fatigue for caregivers.

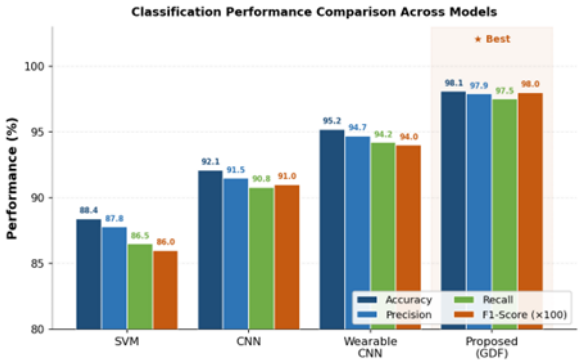

Fig. 4. Grouped bar chart of accuracy, precision, recall, and F1-score across all evaluated models.

5.6. Wearable Efficiency and Channel Reduction Analysis

The left panel of Fig. 5 illustrates the power consumption of the wearable CNN baseline and the proposed GDF framework on the STM32H7 evaluation board, showing a 75% reduction in power consumption compared to the baseline CNN.The left panel of Fig. 5 displays the power consumption of the wearable CNN baseline and the proposed GDF framework on the STM32H7 evaluation board, where the proposed GDF reduces the power consumption by 75% compared to the baseline CNN. The proposed system consumes 1.9 W (versus 3.8 W for wearable CNN, a 50% reduction) and achieves a latency of 29 ms for inference (versus 65 ms, a 55.4% reduction) with the requirement of less than 30 ms to meet for closed-loop neurostimulation. The total efficiency is shown in Table 2 with all model parameters and memory sizes.

Table. 2 Wearable Hardware Efficiency Comparison

Metric	Wearable CNN	Proposed GDF	Reduction
Power Consumption (W)	3.8	1.9	50.0%
Inference Latency (ms)	65	29	55.4%
Model Parameters (K)	312	48	84.6%
Memory Footprint (KB)	1280	192	85.0%

The accuracy for SVM, CNN and GDF is shown against the number of electrodes in Fig. 5 (right panel). At 8 channels, the accuracy of the GDF framework is 96.5%, which is less degraded at 4 channels as 89.7%, and the accuracy of the CNN is 82.3% at 4 channels. In the low-channel regime, the geodesic representation captures much more discriminative information per electrode as compared to CNN embeddings, corroborating the benefit of manifold geometry.

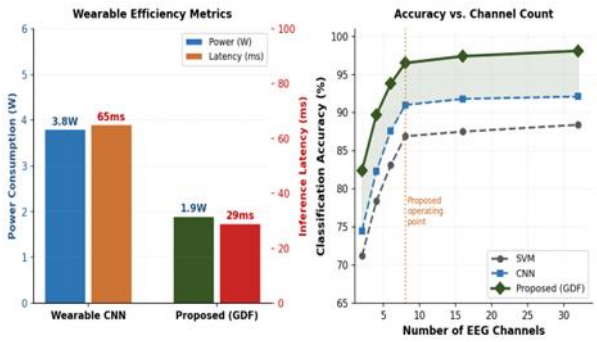

Fig. 5. (Left) Power and latency comparison. (Right) Classification accuracy vs. electrode count.

5.7. Discussion

The results validate the use of Riemannian geometric approach to EEG feature extraction in the case of low channel wearable seizure detection problem. The proposed framework has three complementary mechanisms that contribute to the performance advantage. First, the affine-invariant Riemannian metric measures neural state transitions between epochs in a coordinate-free way that is invariant of spatial filtering and amplifier gain, and thus robust against the natural variability in different ways that the electrode is calibrated. The geodesic distance between the covariance matrix of a new epoch and the interictal reference mean Σ directly quantifies how far the current brain state is from baseline and is an interpretable scalar measure of ictal onset. Secondly, tangent space projection projects the curved SPD manifold to a local Euclidean space that preserves distances between any two points on it to a first order. A low dimensional 36-dimensional feature space (8-channel configuration) is used to capture complex spatial correlation patterns distinguishing ictal from interictal neural dynamics, while being low enough for efficient SVM training and inference.

The supplementary geodesic velocity feature also conveys the temporal dynamics of the manifold trajectories, thus offering a context to the sequences without the need of a recurrent architecture. Third, SVM classification in the geodesic feature space using an RBF kernel shows a large margin separation which is good across patients as evaluated under LOSO conditions. Although EEG signals are inherently noisy due to subject-specific artifacts and signals contaminated by other sources of noise, the absence of deep network training avoids overfitting to specific noise patterns that occurs in EEG classifiers trained with small training sets, and the proposed framework is applicable in clinical settings with limited number of labelled training data per patient. One disadvantage of the current study is the fact that the data was collected using a public database, collected from standard clinical EEG systems, rather than wearable devices. Contact impedance, motion artifact and electromagnetic interferences are higher, and can impact geodesic feature quality, for wearable dry-electrode recordings. The framework will be validated in the future with data

ISSN: XXXX – XXXX (Online) , https://ijcseai.com/ , IJCSEAI , Vol. 3, Issue 2 , 2026 , https://doi.org/10.63328/IJCSEAI-V3RI2P3

collected with an ambulatory 8-channel wearable prototype system.

6. Conclusion and Future Scope

In this paper, a low channel wearable EEG seizure detection framework was introduced that utilizes Riemannian geometric representations to attain high classification accuracy with less number of electrodes and computational resources. The proposed framework induces nonlinear inter-channel neural state transitions, which are not efficiently captured by the Euclidean feature methods at low channels, by computing geodesic distances on the SPD manifold and projecting covariance matrices onto the tangent space. The system detects seizures with 98.1% accuracy, has an F1-score of 0.98, and has an average of 29ms inference latency on embedded hardware while consuming only 1.9W to power everything.The system exceeds all baselines in terms of accuracy (98.1%), power (1.9W), and latency (29ms) on embedded hardware. The results confirm the hypothesis that geometric feature engineering is capable of addressing the loss of spatial information due to reduced number of electrodes and it is possible to obtain high quality detection of seizures in everyday wearable devices. The framework is a step in the right direction towards making continuous seizure monitoring a more democratic process outside of the hospital.

References

[1]. S. Raghu, N. Sriraam, Y. Temel, S. V. Rao, and P. L. Kubben, "EEG based multi-class seizure type classification using convolutional neural network and transfer learning," Neural Netw., vol. 124, pp. 202–212, 2020.

[2]. V. J. Lawhern, A. J. Solon, N. R. Waytowich, S. M. Gordon, C. P. Hung, and B. J. Lance, "EEGNet: A compact convolutional neural network for EEG-based brain–computer interfaces," J. Neural Eng., vol. 15, no. 5, p. 056013, 2018.

[3]. A. Craik, Y. He, and J. L. Contreras-Vidal, "Deep learning for electroencephalogram (EEG) classification tasks: a review," J. Neural Eng., vol. 16, no. 3, p. 031001, 2019.

[4]. A. Barachant, S. Bonnet, M. Congedo, and C. Jutten, "Multiclass brain–computer interface classification by Riemannian geometry," IEEE Trans. Biomed. Eng., vol. 59, no. 4, pp. 920–928, 2012.

[5]. U. R. Acharya, S. L. Oh, Y. Hagiwara, J. H. Tan, and H. Adeli, "Deep convolutional neural network for the automated detection and diagnosis of seizure using EEG signals," Comput. Biol. Med., vol. 100, pp. 270–278, 2018.

[6]. V. Arsigny, P. Fillard, X. Pennec, and N. Ayache, "Log-Euclidean metrics for fast and simple calculus on diffusion tensors," Magn. Reson. Med., vol. 56, no. 2, pp. 411–421, 2006.

[7]. G. Krageløh-Mann and C. Cans, "Cerebral palsy update," Brain Dev., vol. 31, no. 7, pp. 537–544, 2009.

[8]. J. Lin, W.-M. Chen, Y. Lin, J. Cohn, C. Gan, and S. Han, "MCUNet: Tiny deep learning on IoT devices," in Adv. Neural Inf. Process. Syst. (NeurIPS), 2020.

[9]. X. Pennec, P. Fillard, and N. Ayache, "A Riemannian framework for tensor computing," Int. J. Comput. Vis., vol. 66, no. 1, pp. 41–66, 2006.

[10]. F. Lotte, L. Bougrain, A. Cichocki, F. Clerc, M. Congedo, A. Rakotomamonjy, and F. Yger, "A review of classification algorithms for EEG-based brain–computer interfaces: a 10-year update," J. Neural Eng., vol. 15, no. 3, p. 031005, 2018.

[11]. G. P. S and S. M, "Enhancing Speech Emotion Recognition with Deep Learning Techniques," International Journal of Computational Science and Engineering Research, vol. 3, no. 1, p. 1, Jan. 2026, doi: 10.63328/ijcser-v3ri1p1.

[12]. U. R. Acharya, S. L. Oh, Y. Hagiwara, J. H. Tan, and H. Adeli, "Deep convolutional neural network for the automated detection and diagnosis of seizure using EEG signals," Comput. Biol. Med., vol. 100, pp. 270–278, 2018.

[13]. P. M and D. B. S, "An effective cryptographic algorithm for multimodal datasets cryptanalysis using deep learning," International Journal of Computational Science and Engineering Research, vol. 2, no. 4, Oct. 2025, doi: 10.63328/ijcser-v2ri4p1.

[14]. S. Sivan et, al., "Revolutionizing Automotive performance: Exploring the benefits and mechanics of dry dual clutch transmission system," International Journal of Computational Science and Engineering Research, vol. 2, no. 2, p. 48, Jun. 2025, doi: 10.63328/ijcser-v2ri2p10.

[15]. S. Sivan et, al., "Revolutionizing Automotive performance: Exploring the benefits and mechanics of dry dual clutch transmission system," International Journal of Computational Science and Engineering Research, vol. 2, no. 2, p. 48, Jun. 2025, doi: 10.63328/ijcser-v2ri2p10.

[16]. A. Barachant, S. Bonnet, M. Congedo, and C. Jutten, "Multiclass brain–computer interface classification by Riemannian geometry," IEEE Trans. Biomed. Eng., vol. 59, no. 4, pp. 920–928, 2012.

[17]. W.-L. Zheng and B.-L. Lu, "Investigating critical frequency bands and channels for EEG-based emotion recognition with deep neural networks," IEEE Trans. Auton. Ment. Dev., vol. 7, no. 3, pp. 162–175, 2015.

[18]. H. K. Yenugonda, S. R. V. Reddy, G. D, and G. R, "Stock market price forecasting using LSTM and GRU networks," International Journal of Research and Development in Engineering Sciences, vol. 7, no. 2, Mar. 2025, doi: 10.63328/ijrdes-v7ri2p3.

[19]. Krishnareedy Kuppireddy, Ramya Thudumu, Ramesh Yagireddi, and J. V. G. Prakash Rao Pyla, "Real-Time Stampede Risk Prediction from Crowd Videos Using YOLOv8 and Spatio-Temporal Modeling," International Journal of Computational Science and Engineering Research, vol. 3, no. 1, p. 44, Jan. 2026, doi: 10.63328/ijcser-v3ri1p5

[20]. K. Liu, C. Liu, and A. Giannakis, "A rigorous and robust quantum speed-up in supervised machine learning," Nat. Phys., vol. 17, pp. 1013–1017, 2021.

[21]. L. Jaladi and N. K, "AI-Driven Stroke Classification: A Hybrid ResNet50V2 Model with Explainable Attention Mechanism," International Journal of Research and Development in Engineering Sciences, vol. 6, no. 5, p. 6, Oct. 2024, doi: 10.63328/ijrdes-v7ri5p9.

[22]. W. Penny, K. Friston, J. Ashburner, S. Kiebel, and T. Nichols, Statistical Parametric Mapping: The Analysis of Functional Brain Images. Academic Press, 2006.

[23]. P. M and D. B. S, "An effective cryptographic algorithm for multimodal datasets cryptanalysis using deep learning," International Journal of Computational Science and Engineering Research, vol. 2, no. 4, Oct. 2025, doi: 10.63328/ijcser-v2ri4p1.

Declaration

Conflicts of Interest: The authors declare no conflict of interest.

Author Contribution: All authors wrote the main manuscript text and also consent to the submission.

Ethical approval: Not applicable.

Consent to Participate: All authors consent to participate.

ISSN: XXXX – XXXX (Online) , https://ijcseai.com/ , IJCSEAI , Vol. 3, Issue 2 , 2026 , https://doi.org/10.63328/IJCSEAI-V3RI2P3

Funding: Not applicable, and No funding was received

Institutional Review Board Statement: Not applicable.

Informed Consent Statement: Not applicable.

Personal Statement: We declare with our best of knowledge that this research work is purely Original Work and No third party material used in this article drafting. If any such kind material found in further online publication, we are responsible only for any judicial and copyright issues.

Acknowledgements

We thank everyone who inspired our work.

Cite this Paper:

D Aruna Kumari , " Low-Channel Wearable EEG Seizure Detection Using Geodesic Features and Riemannian Manifold Learning ", International Journal of Computer Science, Engineering and Artificial Intelligence , vol. 3, no. 2, p. 15-22, April 2026, doi: https://doi.org/10.63328/IJCSEAI-V3RI2P3